Kovove Mater. 61 2023 81–90
DOI: 10.31577/km.2023.2.81

High-cycle fatigue and tensile strength of AZ91 Mg alloy with MAO-epoxy duplex coating

Filiz Karabudak*

Department of Mechanical Engineering, Faculty of Engineering and Natural Sciences, Gümüşhane University, 2900, Gümüşhane, Turkey

Received 15 May 2022, received in revised form 9 February 2023, accepted 14 February 2023

Abstract

In this study, an epoxy layer was formed by the immersion process, on the oxide layer grown by the micro-arc oxidation (MAO) treatment of the AZ91 magnesium alloy, using the thin film sealing technology, and its effect on fatigue and tensile stress under high cycle conditions was investigated. The microstructures of the AZ91 base material, MAO/AZ91 and MAO-epoxy/AZ91 samples, which were subjected to high-cycle fatigue tests and uniaxial static tensile tests, were assessed through the scanning electron microscope (SEM), X-ray diffraction (XRD) mechanical tests, and fatigue and tensile tests. As a result, the MAO-epoxy duplex coating, which has a homogeneous and compact structure, was observed to improve the fatigue limit value/life, yield strength, ultimate tensile strength, and percentage elongation values of the base material significantly.

K e y w o r d s: AZ91, epoxy, fatigue, MAO, tensile properties

1. Introduction

The AZ91 magnesium alloy, which is used in industries and whose mechanical and corrosion behavior has been extensively researched before, is the most popular magnesium alloy within the AZ group. Magnesium alloys are widely used in aerospace, electronics, communication, and automotive industries since they have good mechanical properties such as good corrosion resistance (for the high-purity version of the alloy), excellent pourability, low density, high specific strength and good thermal conductivity, along with low production costs. In addition to advantages, the alloy also has some disadvantages, such as poor formability, limited ductility, and weak mechanical properties [1–3]. The structural components of the magnesium alloy, which are used in automobiles, aeroplanes, and trains and subjected to cyclic loading, can inevitably lead to destructive fatigue failure. Therefore, the fatigue behavior of magnesium alloys needs to be investigated inclusively [4, 5].

Studies on improving the fatigue behavior of light metals such as Mg have recently focused on surface coating methods [6, 7]. Micro-arc oxidation (MAO) is one of the most popular methods [6, 8]. The electrochemical MAO process, which can increase the film thickness with variable process parameters, provides high wear resistance and corrosion protection [6, 9–11]. In their study, Němcová et al. (2014) concluded that the effect of the MAO treatment of AZ61 on fatigue limit resulted in a 38 % reduction in air and 56 % in a 3.5 % NaCl solution [12]. It is thought that defects in surface coatings can easily lead to the onset of fatigue cracks in existing surface treatments [7]. Therefore, it is assumed that a surface with low roughness should be created to significantly improve the fatigue resistance of Mg alloys.

Srinivasan et al. (2009) evaluated the cracking of the layer formed by MAO treatment with the tensile test under the slow strain rate testing (SSRT) of the AM60 alloy, a cast magnesium alloy. As a result of the slow strain rate testing conditions, they concluded that the stress corrosion cracking (SCC) behavior of the MAO-coated samples caused the base material to crack due to the existence and development of microcracks in the coating [13]. The high porosity content in the MAO coating and large pores were held responsible for the significant reduction in the mechanical

*Corresponding author: e-mail address: filizkarabudak@gumushane.edu.tr

Table 1. Chemical composition and physical properties of AZ91 alloy

AZ91	Chemical composition (wt.%)		Physical properties
Al	8.84	Density	1.80 g cm^{-3}
Zn	0.61	Hardness	63 HB
Mn	0.18	Melting point	615 °C
Si	0.02	Tensile strength	230 MPa
Cu	0.005	Yield strength	150 MPa
Mg	Balance		

properties of magnesium. Sun (2019) investigated the effect of micro-arc oxidation coating on tensile properties in the die-cast AZ91 Mg alloy. The tensile test results indicated that MAO coating decreased the UTS and YS of 2- and 6-mm samples but slightly increased the tensile properties of the 10-mm sample. SEM analysis revealed that differences in the size and content of the pores between the base and the ceramic coating should be responsible for the change in tensile properties [14]. In light of this information, it can be mentioned that there are few studies on increasing the tensile strength of Mg alloys by improving their surface properties with the MAO technique.

In this sense, to improve tensile and fatigue resistance, it is necessary to change/damp the direction of the tip of the growing crack or prevent the growth of the cracks originating from predictable sources. It is possible to improve tensile strength by applying surface coating processes, such as MAO, which form an oxide coating with high strength, to ductile materials that are tougher than brittle materials, and obtaining tougher surfaces resistant to plastic deformation. However, since the porous structure of MAO quickens the onset of the first crack, it is thought that this problem can be solved by filling pores with high-strength epoxy with a second coating (duplex) and ensuring mechanical interlocking with the base material.

This study aimed to increase the fatigue crack initiation time of the base material by decreasing the surface porosity with a second coating on the porous MAO coating grown on the base material. To this end, samples with MAO-epoxy duplex coating were subjected to fatigue and tensile tests, and the limit values were discussed.

2. Experimental procedures

The AZ91 magnesium alloy, whose chemical composition and physical properties are presented in Table 1, was used in this study. The surface of the fatigue and tensile samples prepared in the dimensions given in Fig. 1 was sanded with 800–1200 SiC sandpaper, cleaned with alcohol, and made ready for MAO coating. The DC power supply produced by Faraday Electronics was used in the MAO coating growing process on the base material. In the coating process, a stainless-steel chamber was treated as a cathode, and the AZ91 alloy was treated as an anode. The treatment took 15 min at a constant current density of 100 mA cm^{-2} and a frequency of 300 Hz. Table 2 shows the electrolyte used in the coating process. At the end of the process, MAO-coated samples were washed with distilled water and dried in dry, hot air. To apply the second layer, a two-component DTE 1200 epoxy resin /DTS 1151 hardener epoxy resin system with 100/27 % by weight, provided by Duratek Protective Materials Ltd. Şti. (Turkey), [15] was used [16]. MAO-coated base materials were immersed in the epoxy solution for 10 s, removed for 2–3 s, and reimmersed in the epoxy solution. This process was re-

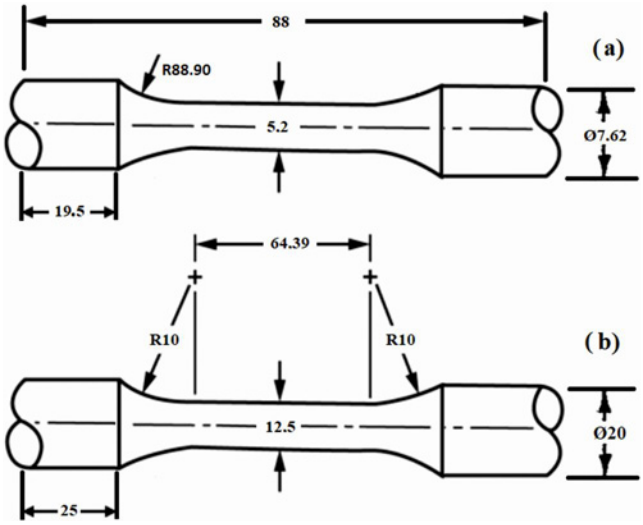

Fig. 1. A sample for (a) fatigue tests and (b) tensile tests (dimensions in mm).

Table 2. Electrolyte composition used for MAO coating

Chemical compound	Weight (g)
K_2SnO_3	1
KOH	1
Na_2HPO_4	3
Na_2SiO_3	4

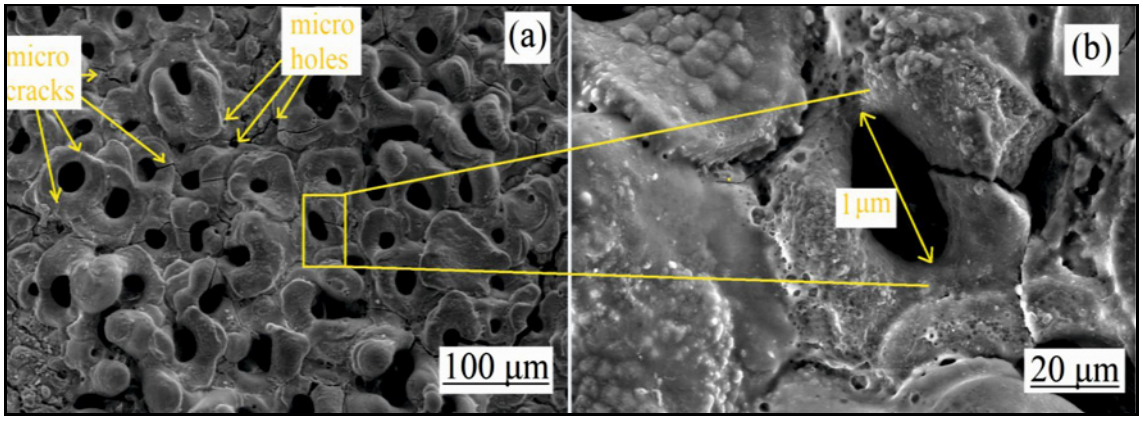

Fig. 2. Surface morphology of the MAO sample at different magnifications: (a) 100 µm and (b) 20 µm.

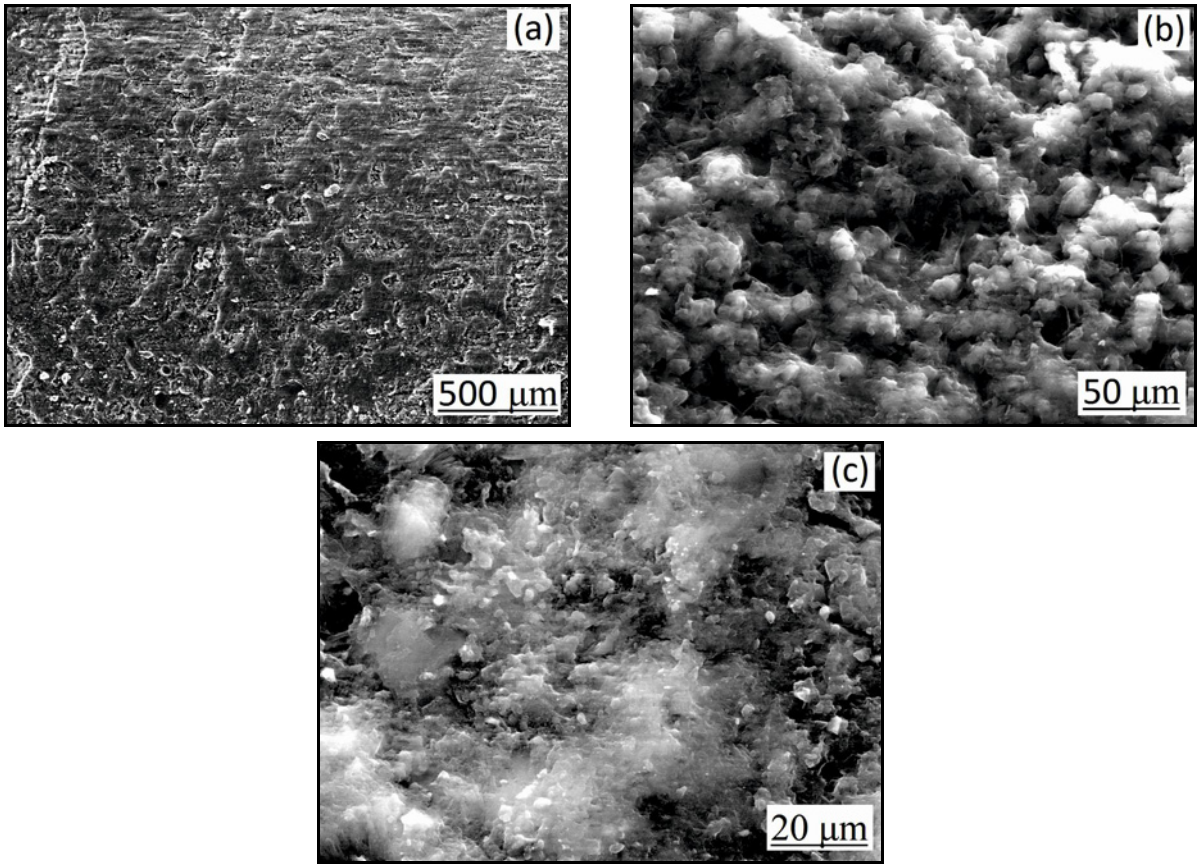

Fig. 3. SEM image of the MAO-epoxy sample at different magnifications: (a) 500 µm, (b) 50 µm, and (c) 20 µm.

peated five times for all samples. MAO-epoxy samples were dried at ambient temperature for 10 days.

Microstructural properties were analyzed by the scanning electron microscope (SEM), with phase distribution within the scanning range of 20–90°, at a 0.1-degree scanning step and 2.5 degree min^{-1} scanning speed, with $\lambda = 1.5404$ Å Cu-Kα-induced X-ray diffraction (XRD). Surface roughness (Ra) values of the coatings were determined using a surface profilometer. Tensile tests were carried out at room temperature using a Shimadzu AGS-X universal test machine with a tensile speed of 0.5 mm min^{-1}. Three tensile test samples were prepared from each of the AZ91 base material, MAO and MAO-epoxy samples (Fig. 1b). High-cycle fatigue tests were conducted in an R. R. Moore-type rotary bending fatigue tester with a rotational speed of 3000 rpm. Three fatigue tests were executed at one stress level to obtain more accurate values in each of the base material, MAO and MAO-epoxy samples (Fig. 1a).

A type B curved fatigue test sample was selected according to the ASTM [17] standard. The specimen dimensions are given in the figure. Tensile test samples were prepared according to the ASTM E8 standard [18, 19].

3. Results and discussion

Figure 2 shows the SEM images related to the surface morphology of the MAO coating. As seen in the figure, the surface morphology of the MAO film has circular [20] pores in micrometric sizes. Typical molten oxide nodules [21] are observed on the surface as in electrochemically coated samples. Micropores result from gas bubbles and micro discharges [22]. The pore diameter in the oxide layer was measured to be about 1 µm. The average of three surface profiles at a measurement distance of 17.5 mm from the coating surface was taken, the average *Ra* value was obtained as 8.27 µm, and the maximum *Rz* value was obtained as 41.0 µm. The measured roughness value was evaluated, considering 5 % margin of error.

Upon examining the SEM images of the MAO-epoxy duplex coating in Fig. 3, no apparent defects are observed on the transparent, smooth, homogeneous, and compact coating surface. The average of three surface profiles at a measurement distance of 17.5 mm from the coating surface was taken, the average *Ra* value was obtained as 0.138 µm, and the maximum *Rz* value was obtained as 0.703 µm. The epoxy resin was seen to fill the thermal cracks and micropores and minimize the surface roughness with a homogeneous, compact, thin film layer that did not contain apparent defects and adhered to the oxide surface very well.

Figure 4 presents the sectional images of MAO and MAO-epoxy duplex coating. In Fig. 4a, coatings grown with the MAO technique consist of three layers. The first layer is outer porous layer, called MAO technological layer. The second is the MAO main functional layer, and the third is the MAO barrier layer. The region between the coating and the substrate is the barrier (transition) layer and is strongly bonded to the substrate. The main functional layer has a more perfect structure and fewer pores than the outermost technological layer. The technological outer layer, which has a very porous and fragile structure, was removed by fine polishing with diamond paste after coating. Here, MAO pre-treatment ensured higher coating adhesion by improving the contact area between the epoxy coating and the base material [23, 24]. The thickness of the MAO coating was measured in the range of 14–15 µm, and the thickness of the epoxy coating was measured in the range of 12–13 µm. The porous and rough MAO layer was evenly filled with epoxy coating, as shown in Fig. 4b. The epoxy coating on the crater-like porous structure of the MAO layer with sealing technology enabled good mechanical interlocking with the magnesium substrate. With the combination of oxide and epoxy coating, the weakness of the MAO coating caused by the porosity on its surface was observed to be eliminated.

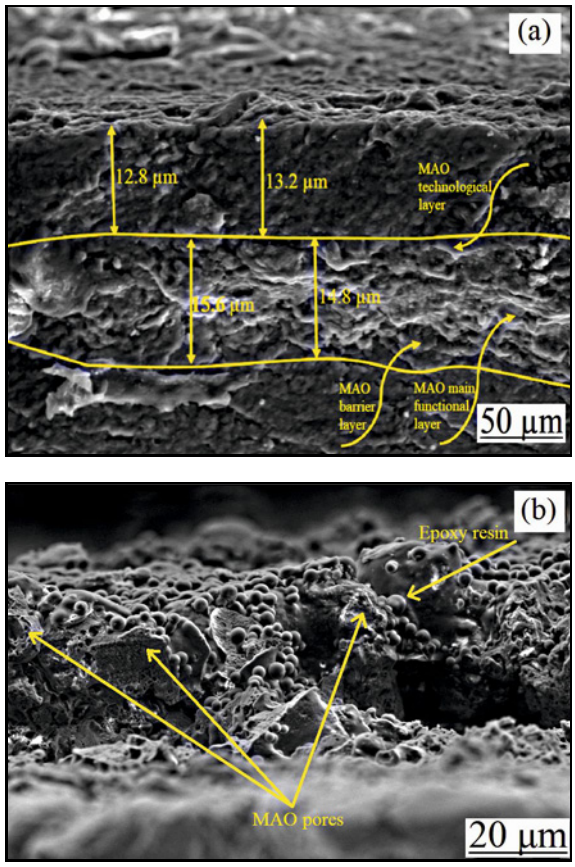

Fig. 4. Cross-sectional view of (a) MAO coating thickness and layers, (b) MAO-epoxy duplex coating.

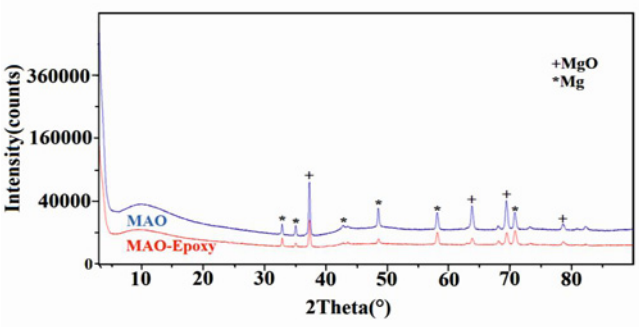

Fig. 5. XRD patterns of MAO and MAO-epoxy coatings.

Figure 5 shows the XRD patterns of MAO and MAO-epoxy coatings. In the curve shown in blue, the dominant peak in the MAO coating grown on the AZ91 Mg alloy is caused by the MgO phase, in par-

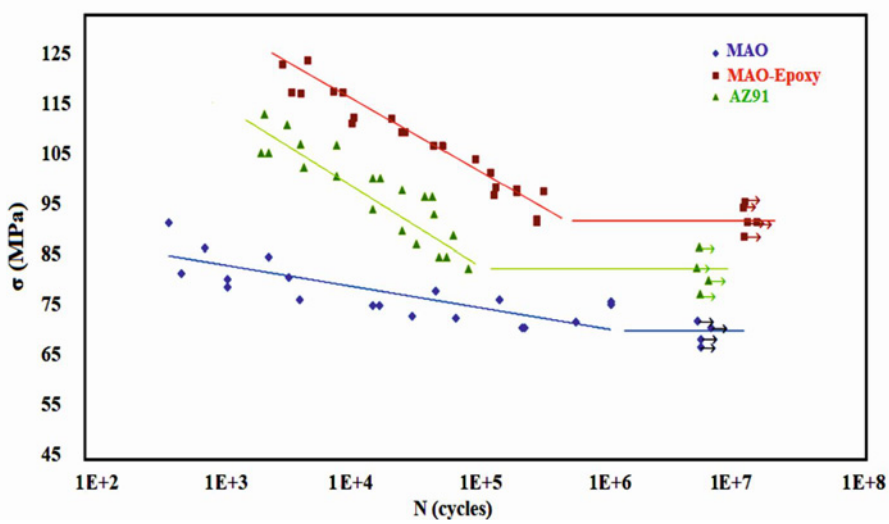

Fig. 6. High cycle S-N curves of samples.

allel with the literature [25–27]. Mg atoms originating from the base material also peak [25, 28]. MgO and Mg peaks originate from the MAO coating and base material [29, 30]. Diffraction peaks in MAO-epoxy coating are absent due to the amorphous structure of the epoxy resin.

3.1. Fatigue test

Figure 6 shows the stress amplitude (σ_a) and the number of cycles to failure (S-N) curves of AZ91 base material, MAO, and MAO-epoxy coatings. Fatigue strength and fatigue life were higher in MAO-epoxy coatings, as expected. The S-N curve of the MAO-epoxy duplex coating exhibits a typical sharp knee, and the σ_a of 92 MPa against 10^7 cycles can be considered the endurance limit. Likewise, the S-N curve of the AZ91 base material exhibits a typical sharp knee. The σ_a of 80 MPa against 10^7 cycles can be considered the endurance limit. The S-N curve of the MAO coating drops continuously with the increasing number of cycles within the broad range of 10^3–10^7 cycles, and the σ_a of 69 MPa against 10^7 cycles can be considered the endurance limit. The endurance limit life was increased by approximately 15 % compared to the AZ91 base material MAO-epoxy duplex coating and decreased by approximately 13 % compared to the MAO coating. The fatigue strength of the MAO coatings decreases compared to the base material since the crack progresses rapidly and results in damage due to the porosity of the MAO structure. In other words, at the endurance limit, the transition of oxide-coated samples to the infinite life zone starts significantly earlier than the uncoated base material due to the inhibition of the cracking onset by the porous oxide layer [6, 31]. When the S-N curves of the MAO-epoxy duplex process in Fig. 6 are examined, the fatigue life and strength of the base material are observed to increase. Here, the endurance limit life increased because MAO pre-treatment improved the contact area between the transparent, smooth, homogeneous, and compact epoxy and the base material and ensured good mechanical interlocking of the epoxy with the magnesium substrate [23, 24].

Experimental results clearly show that MAO coating does not provide any advantages in terms of high-cycle fatigue strength. However, MAO-epoxy duplex coating increases high-cycle fatigue limit and life.

Upon examining Fig. 8 later in the article, it is seen that the yield strength (YS), tensile strength (UTS), and the elongation of the AZ91 base material, MAO oxide coating, and MAO-epoxy duplex coating increase linearly with the fatigue behavior in Fig. 6.

3.1.1. Fatigue fracture surfaces

As is known, the crack propagation process consists of three stages: (I) crack initiation, (II) crack propagation, and (III) destructive deterioration. As seen in Fig. 7, fatigue cracks in MAO-treated samples are assumed to result from stress concentrations at structural defects in the porous oxide layer, supported by a study in the literature [34]. After crack initiation, it tends to a brittle fracture with a "stage III" region over a large area. It is thought that the material tends to harden and brittle as a result of the irreversible plastic deformation caused by repeated stresses and fractures on the contact surface of the AZ91 substrate, which has a ductile tendency, with the MAO coating, supported by studies in the literature [32, 33]. However, since the crack initiation time was faster, the fatigue life was lower than the base material. The broad "stage III" region in Fig. 7c is also supported by the MAO-epoxy curve in Fig. 6, which tends to break with

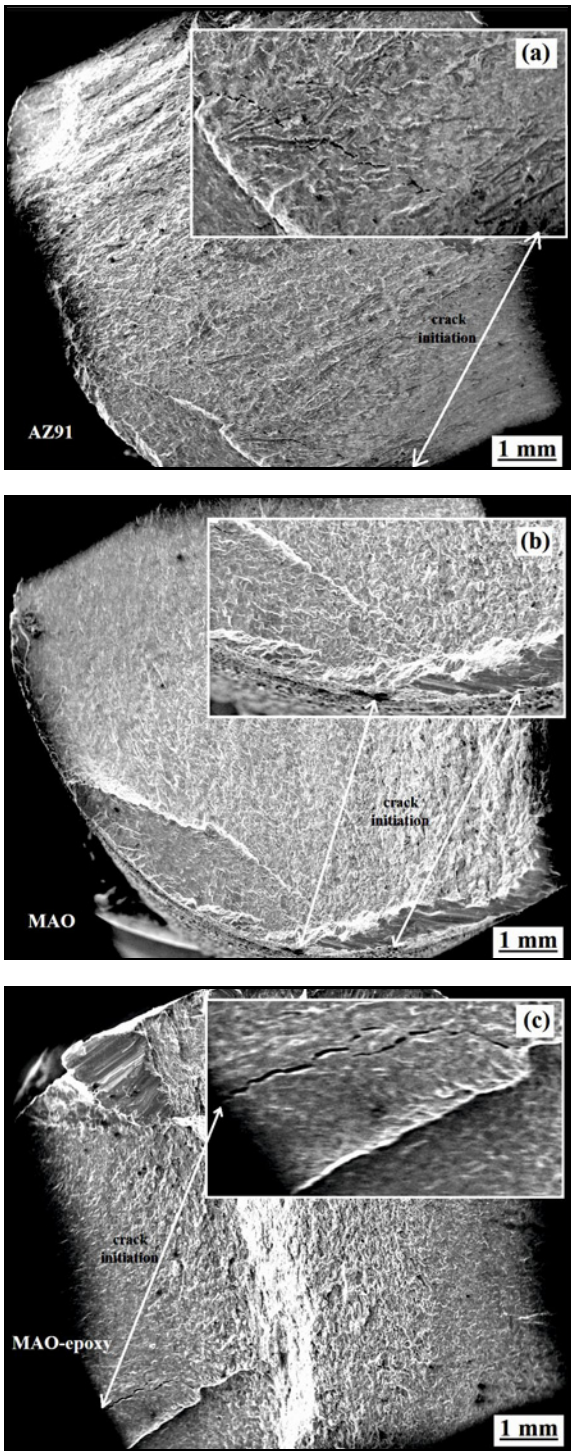

Fig. 7. Fatigue fracture views of (a) AZ91 base material, (b) MAO, and (c) MAO-epoxy samples.

a steep S/N slope. Here, as the bending stress approaches the endurance limit, the strengthening effect of the oxide/epoxy coating becomes quite evident, and it is concluded that it provides a more effective barrier against the development of fatigue cracks. This epoxy barrier layer increased the life of the AZ91 base material.

3.2. Tensile test

Figures 8a,b,c show tensile 'Stress (MPa)/Elongation (%) curves for the AZ91 base material, MAO coating, and MAO-epoxy duplex coating. In Fig. 8d, the tensile stresses in Figs. 8a,b,c are combined in 'Force (N)/Elongation (mm) units. In Fig. 8e, the yield strength (YS), ultimate tensile strength (UTS), and per cent elongation values obtained from these curves as a result of the tensile test are plotted. The MAO porous coating reduced the ultimate tensile strength (UTS) of the base material from 166.824 to 157 MPa, by approximately 6 %. This can be explained by the fact that the possible interaction between the porous MAO coating on the surface causes earlier crack initiation, thus greatly reducing fatigue strength and tensile strength values in parallel to each other (Figs. 7, 9).

MAO-epoxy duplex coating increased the ultimate tensile strength of the base material to 198.966 MPa by approximately 19 %. MAO coating reduced the base material's yield strength (YS) from 161.953 MPa to 154.319 MPa by approximately 5 %. MAO-epoxy duplex coating increased the yield strength of the base material from 161.953 MPa to 189.694 MPa by approximately 17 %. Considering the percentage elongation values, AZ91, MAO, and MAO-epoxy values are 9.4174, 9.04587, and 10.8989 %, respectively.

3.2.1. Tensile fracture surfaces

Figure 9 shows the tensile fracture views of the AZ91 base material, MAO, and MAO-epoxy samples under static load. These samples have ductile fractures on roughly 45° tensile planes. The MAO coating sample had a lower strain rate than the base material due to its porous surface. However, the sample with MAO-epoxy duplex coating significantly increased the strain rate by storing higher energy with mechanical interlocking. Upon examining macroscopic fractures in the base material and MAO-coated samples, it can be seen that high strain rates are characteristic of zigzag fractures on the edge surfaces, supported by a study in the literature [35]. On the other hand, the sample with MAO-epoxy duplex coating tends to have a shear fracture on the surface. The ductile fracture was also observed toward the center of the sample. Here, the MAO-epoxy duplex coating, which enabled sealing and surface smoothness with the oxide coating, led to an increase in brittleness on the surface, and the strain rate in fracture increased with the increase in toughness.

4. Conclusions

In this study, the epoxy coating was produced on

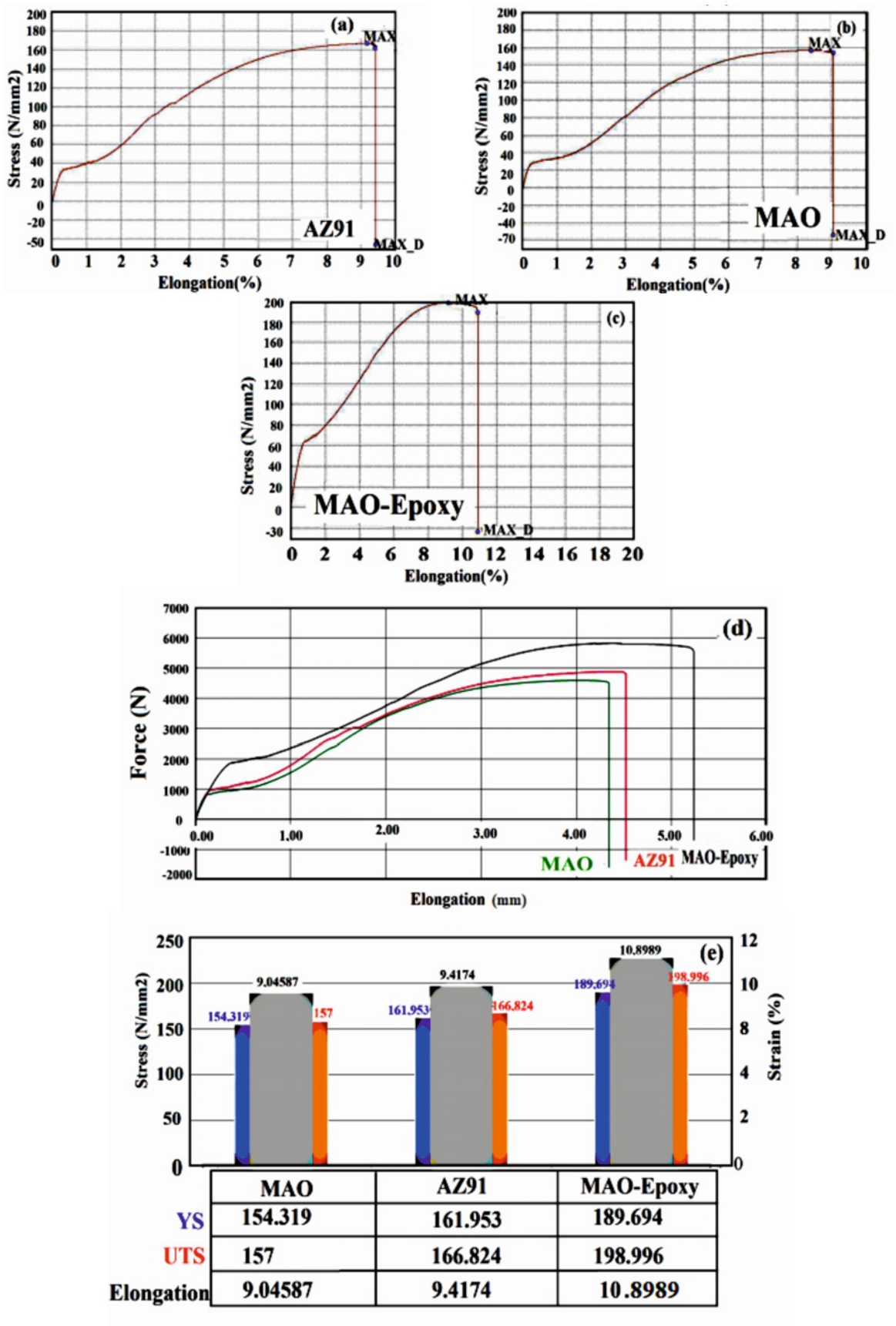

	MAO	AZ91	MAO-Epoxy
YS	154.319	161.953	189.694
UTS	157	166.824	198.996
Elongation	9.04587	9.4174	10.8989

Fig. 8. (a)–(c) Tensile curves (Stress (MPa)/Elongation (%)), (d) combined tensile curves (Force (N)/Elongation (mm)), and (e) YS, UTS and elongation values of AZ91, MAO and MAO-Epoxy samples.

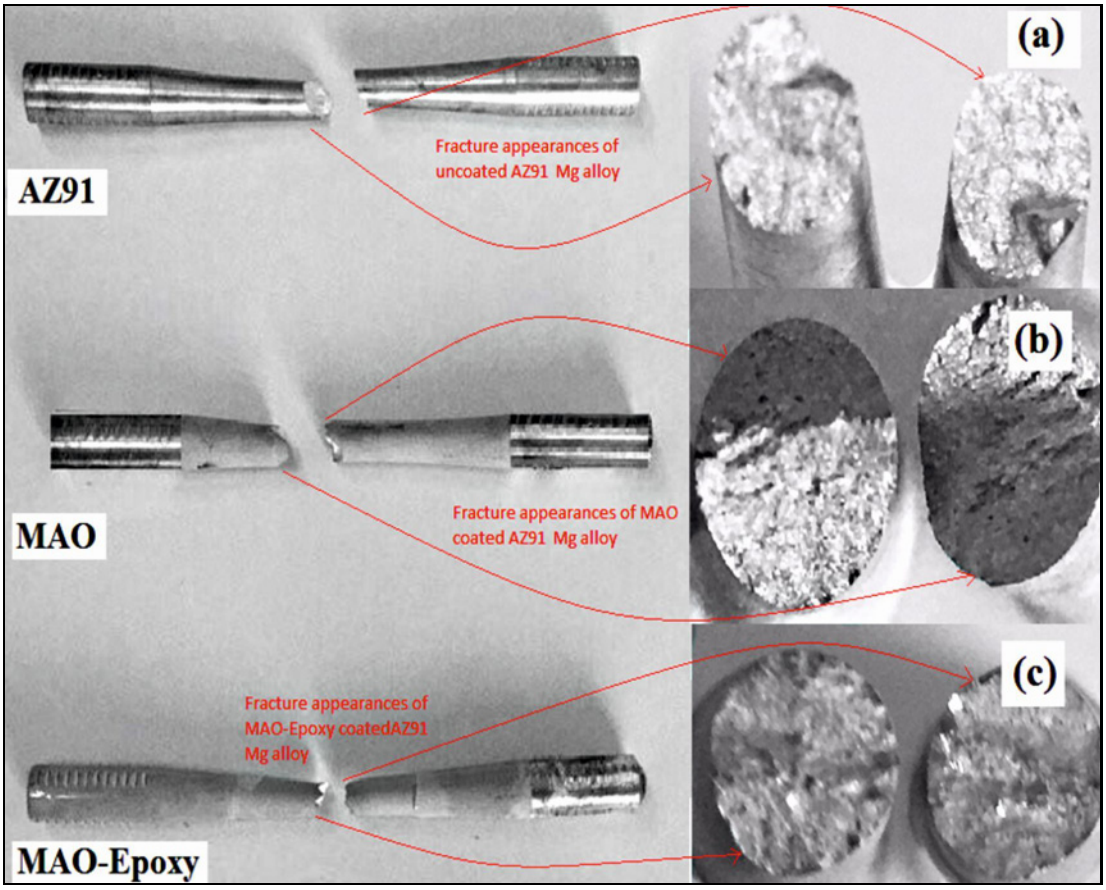

Fig. 9. Tensile fracture views of AZ91, MAO and MAO-epoxy samples.

MAO pre-treated AZ91 Mg alloy samples. Strength values were compared by applying fatigue and tensile tests to AZ91, MAO, and MAO-epoxy samples.

– The oxide layer in the MAO (average *Ra*, 8.27 μm) coating has a high porosity by nature, whereas the epoxy coating in the MAO-epoxy (average *Ra*, 0.138 μm) duplex coating functions as a barrier by transparently filling the crater-like porous structures in the oxide layer, and ensures good mechanical interlocking.

– The results of the fatigue tests revealed that MAO coatings could cause a 13 % reduction in the endurance limit of the base material. Upon comparing the MAO-epoxy coating and base material, a 15 % significant increase in the fatigue limit life is observed.

– When the AZ91 base material is coated with MAO, UTS decreases by 6 % and YS by 5 %; when MAO-epoxy is coated, UTS increases by 19 % and YS by 17 %.

– When the per cent elongation values of "MAO-epoxy (10.8989) > AZ91 (9.4174) > MAO (9.04587)" are considered, it is seen that MAO-epoxy has the highest per cent elongation value.

– The fatigue strengths of the AZ91 base material, MAO, and MAO-epoxy coatings are linearly proportional to yield strength (YS), ultimate tensile strength (UTS), and percentage elongation.

– As a result, since the porous MAO coating, which reduces the fatigue and tensile strength of the AZ91 base material, is mechanically locked with epoxy, which is compact and has low surface roughness without obvious defects on the surface, the fatigue crack initiation time and crack propagation rate decrease, fatigue strength increases, and tensile properties improve.

References

[1] D. Ni, D. Wang, A. Feng, G. Yao, Z. Ma, Enhancing the high-cycle fatigue strength of Mg-9Al-1Zn casting by friction stir processing, Scripta Materialia 61 (2009) 568–571. https://doi.org/10.1016/j.scriptamat.2009.05.023

[2] F. Fintová, L. Kunz, Cyclic plastic behavior and fatigue life of AZ91 alloy in as-cast and ultrafine grained state, Materials Engineering 21 (2014) 109–115.

[3] P. Kumar, L. Thakur, N. Bhadouria, S. Dixit, Microstructure and mechanical behaviour of friction stir processed AZ91-D magnesium alloy – optimization of process parameters by using the Taguchi method, Kovove Materialy-Metallic Materials 57 (2019) 207–217. https://doi.org/10.4149/km_2019_3_207

[4] F. Hnilica, V. Očenášek, I. Stulíková, B. Smola, The effect of structure defects on the fatigue behaviour of AZ91 magnesium alloy prepared by sand casting and squeeze casting, Kovove Materialy-Metallic Materials 43 (2005) 300–316.
[5] Y. Lin, X. Chen, Z. Liu, J. Chen, Investigation of uniaxial low-cycle fatigue failure behavior of hot-rolled AZ91 magnesium alloy, International Journal of Fatigue 48 (2013) 122–132. https://doi.org/10.1016/j.ijfatigue.2012.10.010
[6] A. Yerokhin, A. Shatrov, V. Samsonov, P. Shashkov, A. Leyland and A. Matthews, Fatigue properties of Keronite® coatings on a magnesium alloy, Surface and Coatings Technology 182 (2004) 78–84. https://doi.org/10.1016/S0257-8972(03)00877-6
[7] B. J. Wang, S. Wang, D. Xu, E. Han, Recent progress in fatigue behavior of Mg alloys in air and aqueous media: A review, Journal of Materials Science & Technology 33 (2017) 1075–1086. https://doi.org/10.1016/j.jmst.2017.07.017
[8] A. Morri, L. Ceschini, C. Martini, A. Bernardi, Influence of plasma electrolytic oxidation on fatigue behaviour of ZK60A-T5 magnesium alloy, Coatings 10 (2020) 1180. https://doi.org/10.3390/coatings10121180
[9] Y. Zhang, Y. Chen, H. Q. Du, Y. W. Zhao, Corrosion resistance of micro-arc oxidation coatings formed on aluminum alloy with addition of Al_2O_3, Materials Research Express 5 (2018) 036527. https://doi.org/10.1088/2053-1591/aab732
[10] L. Famiyeh, X. Huang, Plasma electrolytic oxidation coatings on aluminum alloys: Microstructures, properties, and applications, Modern Concepts in Material Science 2 (2019) 1–13. https://doi.org/10.33552/MCMS.2019.02.000526
[11] X. He, H. Liang, Z. Yan, R. Bai, Stress corrosion cracking behavior of micro-arc oxidized AZ31 alloy, Proceedings of the Institution of Mechanical Engineers, Part C: Journal of Mechanical Engineering Science 234 (2020) 1640–1652. https://doi.org/10.1177/0954406219894029
[12] A. Němcová, P. Skeldon, G. Thompson, S. Morse, J. Čížek, B. Pacal, Influence of plasma electrolytic oxidation on fatigue performance of AZ61 magnesium alloy, Corrosion Science 82 (2014) 58–66. https://doi.org/10.1016/j.corsci.2013.12.019
[13] P. B. Srinivasan, C. Blawert, W. Dietzel, K. U. Kainer, Stress corrosion cracking behaviour of a surface-modified magnesium alloy, Scripta Materialia 59 (2008) 43–46. https://doi.org/10.1016/j.scriptamat.2008.02.032
[14] Z. Sun, Effect of Plasma Electrolytic Oxidation Coating on Tensile Properties of High Pressure Die Cast Magnesium Alloy AZ91, Ontario: University of Windsor (Canada), ProQuest Dissertations Publishing, 2019.
[15] T. Khan, O. Aydın, V. Acar, M. Aydın, B. Hülagü, H. Bayrakçeken, M. Ö. Seydibeyoğlu, H. Akbulut, Experimental investigation of mechanical and modal properties of Al_2O_3 nanoparticle reinforced polyurethane core sandwich structures, Materials Today Communications 24 (2020) 101233. https://doi.org/10.1016/j.mtcomm.2020.101233
[16] Duratek 1200 Product Data Sheet, Duratek Protective Materials Co. Ltd., 09/11/2021. http://www.duratek.com.tr/tr/urunler/kompozit-icin-urunler/laminasyon-recineleri
[17] R. Swanson, Handbook of Fatigue Testing, Volume 566, Philadelphia: ASTM Committee E-9, 1974.
[18] ASTM, Standard Test Methods for Tension Testing of Metallic Materials, ASTM International, 2013.
[19] H. S. Kumaraswamy, V. Bharat, T. K. Rao, Influence of boron fiber powder and graphite reinforcements on physical and mechanical properties of aluminum 2024 alloy fabricated by stir casting, Journal of Minerals and Materials Characterization and Engineering 7 (2019) 103–116. https://doi.org/10.1016/j.matpr.2018.02.170
[20] K. Rokosz, T. Hryniewicz, Comparative SEM and EDX analysis of surface coatings created on niobium and titanium alloys after plasma electrolytic oxidation (PEO), Tehnički Vjesnik 24 (2017) 465–472. https://doi.org/10.17559/TV-20151105101443
[21] K. Rokosz, T. Hryniewicz, S. Raaen, SEM, EDS and XPS analysis of nanostructured coating formed on NiTi biomaterial alloy by plasma electrolytic oxidation (PEO), Tehnički Vjesnik 24 (2017) 193–198. https://doi.org/10.17559/TV-20151021112657
[22] M. Toorani, M. Aliofkhazraei, R. Naderi, Ceria-embedded MAO process as pretreatment for corrosion protection of epoxy films applied on AZ31-magnesium alloy, Journal of Alloys and Compounds 785 (2019) 669–683. https://doi.org/10.1016/j.jallcom.2018.12.257
[23] X. Lu, X. Feng, Y. Zuo, P. Zhang, C. Zheng, Improvement of protection performance of Mg-rich epoxy coating on AZ91D magnesium alloy by DC anodic oxidation, Progress in Organic Coatings 104 (2017) 188–198. https://doi.org/10.1016/j.porgcoat.2016.11.001
[24] X. Lu, X. Feng, Y. Zuo, C. Zheng, S. Lu, L. Xu, Evaluation of the micro-arc oxidation treatment effect on the protective performance of a Mg-rich epoxy coating on AZ91D magnesium alloy, Surface and Coatings Technology 270 (2017) 227–235. https://doi.org/10.1016/j.surfcoat.2015.02.052
[25] Y. Wang, M. Zheng, K. Wu, Microarc oxidation coating formed on SiCw/AZ91 magnesium matrix composite and its corrosion resistance, Materials Letters 59 (2005) 1727–1731. https://doi.org/10.1016/j.matlet.2005.01.050
[26] R. Rojaee, M. Fathi, K. Raeissi, Electrophoretic deposition of nanostructured hydroxyapatite coating on AZ91 magnesium alloy implants with different surface treatments, Applied Surface Science 285 (2013) 664–673. https://doi.org/10.1016/j.apsusc.2013.08.108
[27] R. Küçükosman, E. E. Şüküroğlu, Y. Totik, S. Şüküroğlu, Investigation of wear behavior of graphite additive composite coatings deposited by micro arc oxidation-hydrothermal treatment on AZ91 Mg alloy, Surfaces and Interfaces 22 (2021) 100894. https://doi.org/10.1016/j.surfin.2020.100894
[28] W. Qudong, L. Yizhen, Z. Xiaoqin, D. Wenjiang, Z. Yanping, L. Qinghua, L. Jie, Study on the fluidity of AZ91 + xRE magnesium alloy, Materials Science and Engineering A 271 (1999) 109–115. https://doi.org/10.1016/S0921-5093(99)00185-9
[29] M. Al-Qadhi, N. Merah, Z. M. Gasem, Mechanical properties and water uptake of epoxy-clay nanocomposites containing different clay loadings, Journal of

Materials Science 48 (2013) 3798–3804.
https://doi.org/10.1007/s10853-013-7180-5

[30] J. S. Sagar, S. J. Kashyap, G. M. Madhu, P. Dixit, Investigation of mechanical, thermal and electrical parameters of gel combustion-derived cubic zirconia/epoxy resin composites for high-voltage insulation, Cerâmica 66 (2020) 86–196.
https://doi.org/10.1590/0366-69132020663782887

[31] K. Hockauf, L. Köhler, M. Handel, T. Halle, D. Nickel, G. Alisch, T. Lampke, The effect of anodic oxide coating on the fatigue behaviour of AA6082 with an ultrafine-grained microstructure, Materialwissenschaft und Werkstofftechnik 42 (2011) 624–631.
https://doi.org/10.1002/mawe.201100837

[32] W. B. Dai, L. X. Yuan, C. Y. Li, D. He, D. W. Jia, Y. M. Zhang, The effect of surface roughness of the substrate on fatigue life of coated aluminum alloy by micro-arc oxidation, Journal of Alloys and Compounds 765 (2018) 1018–1025.
https://doi.org/10.1016/j.jallcom.2018.06.290

[33] W. Dai, C. Li, D. He, D. Jia, Y. Zhang, Z. Tan, Mechanism of residual stress and surface roughness of substrate on fatigue behavior of micro-arc oxidation coated AA7075-T6 alloy, Surface and Coatings Technology 380 (2019) 125014.
https://doi.org/10.1016/j.surfcoat.2019.125014

[34] W. Dai, J. Hao, C. Li, D. He, D. Jia, Y. Zhang, Z. Tan, Residual stress relaxation and duty cycle on high cycle fatigue life of micro-arc oxidation coated AA7075-T6 alloy, International Journal of Fatigue 130 (2020) 105283.
https://doi.org/10.1016/j.ijfatigue.2019.105283

[35] C. D. Lee, K. S. Shin, Effect of microporosity on the tensile properties of AZ91 magnesium alloy, Acta Materialia 55 (2007) 4293–4303.
https://doi.org/10.1016/j.actamat.2007.03.026